Insight into the fergusonite-scheelite phase transition of ABO_4-type oxides by density functional theory: a case study of the subtleties of the ground state of $BiVO_4$

Taifeng Liu[1, 2*], Xingfan Zhang[2], Jingcheng Guan[2], C. Richard A. Catlow[2,3], Aron Walsh[4], Alexey A. Sokol[2*], and John Buckeridge[5*]

1. National & Local Joint Engineering Research Center for Applied Technology of Hybrid Nanomaterials, Henan University, Kaifeng 475004, China
2. Kathleen Lonsdale Materials Chemistry, Department of Chemistry, University College London, 20 Gordon Street, London, WC1H0AJ, United Kingdom
3. School of Chemistry, Cardiff University, Park Place, Cardiff, CF10 1AT, United Kingdom
4. Department of Materials, Imperial College London, London SW7 2AZ, United Kingdom
5. School of Engineering, London South Bank University, 103 Borough Road, London SE1 OAA, United Kingdom

Corresponding authors: T. Liu: uccatl0@ucl.ac.uk; A. Sokol: a.sokol@ucl.ac.uk; J. Buckeridge: j.buckeridge@lsbu.ac.uk

Abstract: $BiVO_4$ (BVO) is an important photocatalytic and ferro-elastic material. It has been extensively studied using density functional theory (DFT). However, on optimisation, at a commonly employed level of theory using the PBE exchange and correlation functional, the monoclinic scheelite (*ms*-BVO) structure transforms to a higher-symmetry tetragonal scheelite (*ts*-BVO) phase spontaneously, which has also been confirmed by other groups. Such a transformation is highly unusual, as one would expect the transition to the lower symmetry structure to be modelled well at this level of theory, as is the case with, for example, the perovskite $BaTiO_3$, and hints at a subtle interplay between structural and electronic properties. In this work, we

demonstrate that this phase transition nevertheless can be described accurately with DFT, but only using a hybrid density functional with ~60% Hartree Fock (HF) exchange. We find a soft phonon mode in *ts*-BVO, which corresponds to the phase transition from *ts*-BVO to *ms*-BVO associated with a double-well potential characterizing this phase transition, implying that the transition is of the second order. We find two key factors that can explain this surprising behaviour. First, the polarizability of the Bi^{3+} ion, with an on-site contribution from the hybridization of its 6s and 6p states, is notably underestimated by DFT. Moreover, the effective radius of the Bi^{3+} ion proves to be too large. With the 60% HF exchange hybrid functional, the description of the polarizability of Bi^{3+} does not improve but the radius of the Bi^{3+} ions approach more realistic values. The polarizability of the O and V ions are reasonably described already by PBE. To gain a further insight into the problem, we investigated the structural stability of other ABO_4 oxides, including $ScVO_4$, $LaNbO_4$, $YTaO_4$, and $CaWO_4$, and related materials. Some of them have a similar behaviour to BVO, whose ground state monoclinic structure proves to be unstable using commonly employed DFT approaches. In particular, for $ScVO_4$, we found that the scheelite tetragonal and fergusonite monoclinic structure cannot be distinguished using the PBEsol functional. But the fergusonite monoclinic structure becomes stable using the hybrid functionals with high fractions of HF exchange, which points at the crucial role of the accurate ionic sizes reproduction by the method of choice as the on-site Sc^{3+} polarizability is too low to have a significant effect. Our findings would be of high interest for the study of other problematic materials with subtle size and polarization

properties, especially ABO_4 oxides that undergo the phase transition from the scheelite tetragonal to fergusonite monoclinic structure.

1. Introduction:

$BiVO_4$ (BVO) has attracted much attention in recent years in photocatalysis and photoelectrochemical water splitting due to its visible light activity, favourable conduction and valence band edge positions, and low-cost facile synthesis route[1-6]. Moreover, it is an important ferro-elastic material[7]. The phase transition between the low temperature ferro-elastic monoclinic scheelite (*ms*-BVO) and the high temperature para-elastic tetragonal scheelite (*ts*-BVO) is also widely investigated[8-11]. Both phases have a crystallographic unit cell of four formula units. At ~ 528 K, the material undergoes a reversible second-order phase transition from *ms*-BVO (space group *I2/a*) to *ts*-BVO (space group $I4_1/a$), in which the primitive unit cell of two formula units transforms as shown in **Figure 1**[12]. This transition is driven by the *q~0* soft optical phonon B_g mode[13].

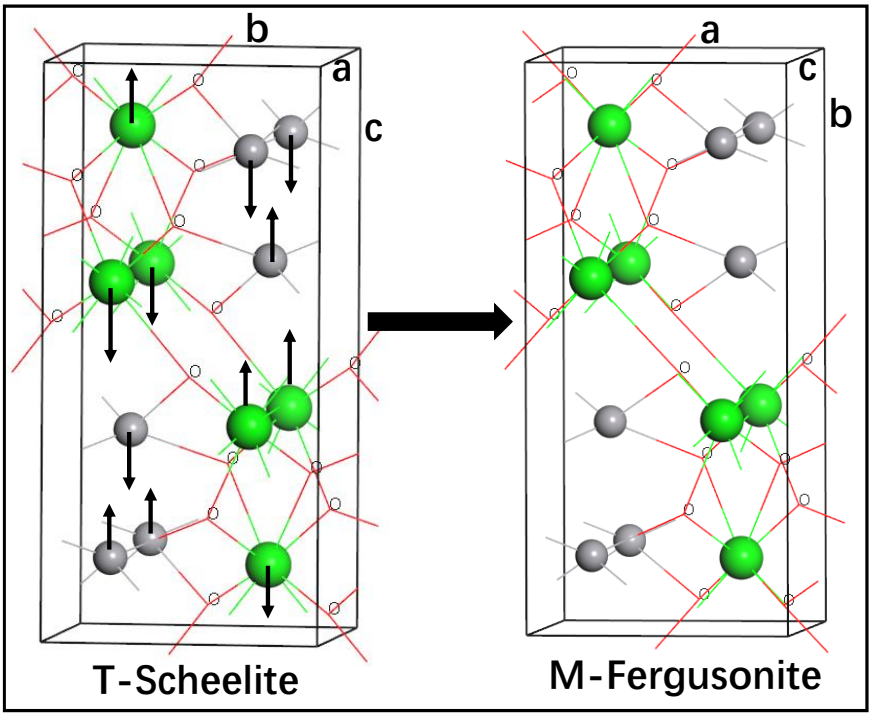

Figure 1. The tetragonal scheelite (T-Scheelite) and monoclinic fergusonite (M-Fergusonite) structures of ABO_4 oxide. Green spheres: A atoms, grey spheres: B atoms, and symbol 'O': O atoms[14]. The displacement along the $T(B_g)$ mode for the phase transition in scheelite are shown with arrows.

BVO is not unique and there are still many other ABO_4 materials having a similar phase transition[15]. The ABO_4 type orthro-niobates are generally observed to adopt the monoclinic (space group I2/a) fergusonite type structure, and the term "fergusonite" is loosely used to describe the monoclinic ABO_4 oxides[16]. In particular, the rare-earth niobates ($LnNbO_4$, Ln=La-Lu) are known to undergo a reversible, pure ferro-elastic phase transition from a high temperature para-elastic, scheelite-type (tetragonal, I41/a) to a ferro-elastic, fergusonite-type (monoclinic, I2/a) structure at low temperature[17-23]. Moreover, it has been also established that in many other chemical

classes of compounds of the ABO_4-type family (vanadates[22, 24-26], tantalates[27], tungstates[14], molybdates[14], etc.) temperature or pressure induces structural transforms from the tetragonal scheelite to monoclinic fergusonite symmetry which is illustrated in Figure 1. The lattice constants of conventional scheelite and fergusonite structures are typically almost the same, as can be seen in the lattice constants of BVO analysed below. A search in the Inorganic Crystal Structure Database (ICSD)[28] produces many large numbers of scheelite and fergusonite structured materials of diverse chemical composition listed in **Table 1**.

Table 1. ABO_4 vanadate, niobate, tantalate, tungstate, and molybdates compounds with scheelite and fergusonite structures

ABO_4 oxides	Scheelite (A ions)	Fergusonite (A ions)
AVO_4	Sc, Y, Sm, Eu, Ho-Lu	Sc, Sm, Eu, Ho, Lu
$ANbO_4$	Y, La-Nd, Sm-Lu	Y, La-Nd, Sm-Lu
$ATaO_4$	Y, Nd, Sm-Er	Y, Nd, Sm-Er
AWO_4	Ca, Sr, Ba, Pb, Eu	Ca, Sr, Ba
$AMoO_4$	Ca, Sr, Ba, Cd, Pb, Eu	Ca, Sr, Ba

Energy differences between the phases related by such structural transformations are usually very small which poses a serious challenge to computational studies. A uniformly accurate reproduction of the relevant parts of the energy landscape is in such cases an important prerequisite, and commonly, Density functional theory (DFT)

has been considered as a reliable method that should guarantee the necessary level of accuracy and is widely applied in materials physics, providing detailed insight into the properties of materials at the atomic level. And, indeed, DFT using semi-local functionals like PBE[29], or hybrid functionals that admix a low fraction (generally within the 20-25% range) of the nonlocal Hartree Fock (HF) exchange, can reproduce, or predict experimentally observed phase transitions in many materials accurately, including textbook perovskite structured $BaTiO_3$ and $SrTiO_3$[30-34]. Some of the scheelite-structured materials listed in **Table 1** have already been investigated using DFT. Mullens *et. al.*[35] found the PBEsol functional works very well for both $SmNbO_4$ and $SmTaO_4$, but a greater discrepancy between the observed and calculated volumes was seen for the latter. The calculated and observed structural properties for $HoNbO_4$ were reproduced best using the PBEsol functional[36], whereas the PBE functional-based calculations provided a better agreement with experiment for both polymorphs (space group I2/a, and P2/c) of $HoTaO_4$[35]. The authors concluded there is no unique universal exchange correlation functional appropriate for these types of oxides. Kuwabara et. al.[37] calculated the lattice constants of tetragonal (t-$LaNbO_4$, I41/a) and monoclinic (m-$LaNbO_4$, I2/c) using local density approximation (LDA) and generalized gradient approximation (GGA) PBE functional. They found the monoclinic phase is more stable than the tetragonal one with LDA. In contrast, the t-$LaNbO_4$ has lower energy than m-$LaNbO_4$ in the GGA PBE functional calculation. Feng et. al.[27] studied the high-temperature phase transition between the tetragonal (scheelite) and monoclinic (fergusonite) forms of $YTaO_4$ using a combination of first-

principles calculations and a Landau free-energy expansion, and they found that the GGA PBE functional works well in this case.

Considering the case of BVO, we found, surprisingly, that both the popular GGA and hybrid level DFT with a low fraction of HF are unable to simulate the phase transition from *ms*-BVO to *ts*-BVO. When optimising the lattice parameters and atomic positions of *ms*-BVO with either of the commonly employed DFT approaches, the monoclinic structure spontaneously transforms to the *ts*-BVO phase. In this paper, we demonstrate that the phase transition from *ms*-BVO to *ts*-BVO can only be reproduced or predicted accurately with a hybrid functional including a large fraction (~60%) of HF and using unusually stringent convergence criteria.[38]. We show that such an approach is essential to model the ground state structure and the high temperature phase transition accurately. This observation may have a direct relevance to the investigation of phase transitions in other materials of the scheelite group, but as already can be seen from the recent work on the niobates and tantalates mentioned above, the method of choice can prove to be specific to each compound. What we can, however, conclude is that the scheelite structure has a unique feature in its sensitivity to the level of accuracy provided by the methodological approach.

Taking into account the computational cost, it is not feasible for us to investigate the whole class of these materials using hybrid functionals under the high convergence criteria, especially some of the rare-earth elements containing *f* electrons and having complex magnetic states. Here, we report a detailed study of the BVO, which is the main topic of our paper, but we also have scrutinised some of

representative scheelite-structured materials using the PBEsol functional focussing on the relative stability (and existence) of the scheelite and fergusonite structures. Furthermore, we have taken $ScVO_4$ as an example and performed more detailed calculations with hybrid functionals. The paper is organized as following: we give the computational details in section 2, present and discuss the results in section 3, and final conclusions are drawn in section 4.

2. Methods Section-Computational details

We carried out DFT calculations using Vienna Ab initio Simulation Package (VASP) code[39-40]. For the material without magnetic moment, such as BVO, we performed non-spin-polarized calculations, but for the materials with magnetic moment, spin-polarized method is used (predictably, running spin-polarised calculations on the BVO structures did not result in any spontaneous spin polarisation.). For the exchange and correlation term, Perdew-Burke-Enzerhof (PBE)[29], PBE revised for solids (PBEsol[36]) and PBE0[41] hybrid functionals were used. We treat the O ($2s^2$, $2p^4$), V ($3p^6$, $4s^2$, $3d^3$), and Bi ($5d^{10}$, $6s^26p^3$) electrons as valence electrons, with the core electrons represented by projector-augmented-wave (PAW) potential. The fraction of exact exchange interaction α in the hybrid functional was varied from 0.25 to 0.7 in order to identify a suitable α value. The electronic wave functions were expanded in a large plane wave basis set with an energy cut-off of 950 eV. Self-consistent DFT energies were converged to 10^{-8} eV per primitive cell, and geometry optimization were deemed converged when the residual forces on the atoms were smaller than 4×10^{-4} eV/ Å. For the 12-atom primitive cell, A 6×6×6 k-point

mesh across the one first Brillouin zone was used. To verify our findings for the *ms*-BVO structure from the plane wave PAW calculations with VASP, full potential all-electron calculations using atomic numerical basis functions were performed employing the PBEsol functional as implemented in the FHI-aims code[42]. The details of the input files including the basis set and relativistic corrections are put in the supporting information (SI).

To compute the phonon frequencies, We have employed the supercell approach as implemented in the Phonopy[43-44] software, using the VASP code as the force calculator. We also used the VASP code itself to calculate the phonon frequencies with α=0.6 in *ts*-BVO to confirm the results produced by Phonopy. Both the VASP code and phonopy use finite difference to determine the Hessian matrix. In phonopy, the displacement amplitude is 0.01 Å. In VASP, each ion is subject to positive and negative displacements of 0.015 Å.

For other materials, the same converge criteria are imposed as for BVO, as the number of atoms in respective unit cells are the same, and lattice constants of all the scheelite and fergusonite structures are similar. The pseudopotential of other materials used in all calculations refer to the materials project[45]. Briefly, there are Sc ($3s^2 3p^6 4s^2 3d^1$), Lu ($3p^6 5d^1 6s^2$), Sm ($5p^6 6s^2 4f^3$), Pr ($5p^6 6s^2 4f^3$), Y ($4s^2 4p^6 5s^2 4d^1$), La ($5s^2 5p^6 6s^2 5d^1$), Ca ($3s^2 3p^6 4s^2$), Nb ($4p^6 5s^2 4d^3$), Ta ($5p^6 6s^2 5d^3$), and W ($5s^2 5p^6 6s^2 5d^4$).

3. Results and discussion

3.1 BVO calculations using PBEsol functional

The initial geometries of the primitive cell of *ms*-BVO and *ts*-BVO were taken

from experiment[11] and summarized in **Table 2**. In the *ms*-BVO, there are four sets of Bi-O bonds and two sets of V-O bonds. In *ts*-BVO, there are two sets of Bi-O bonds and one set of V-O bonds. Using the planewave code VASP, we find that after optimisation with PBEsol functional, *ts*-BVO remains in the tetragonal phase. The optimised geometry is shown in **Figure 2 (a)** and reported in **Table 2** where it is compared with experiment. Both the lattice parameters and bond lengths of Bi-O and V-O remain close to experimental values. After optimisation, we use a 4×4×4 supercell containing 768 atoms to undertake the phonon calculations of *ts*-BVO. The resulting calculated phonon dispersion with the non-analytical term correction is shown in the **Figure 2 (b)**. We note that there are three real acoustic phonon modes and no soft phonon modes in *ts*-BVO.

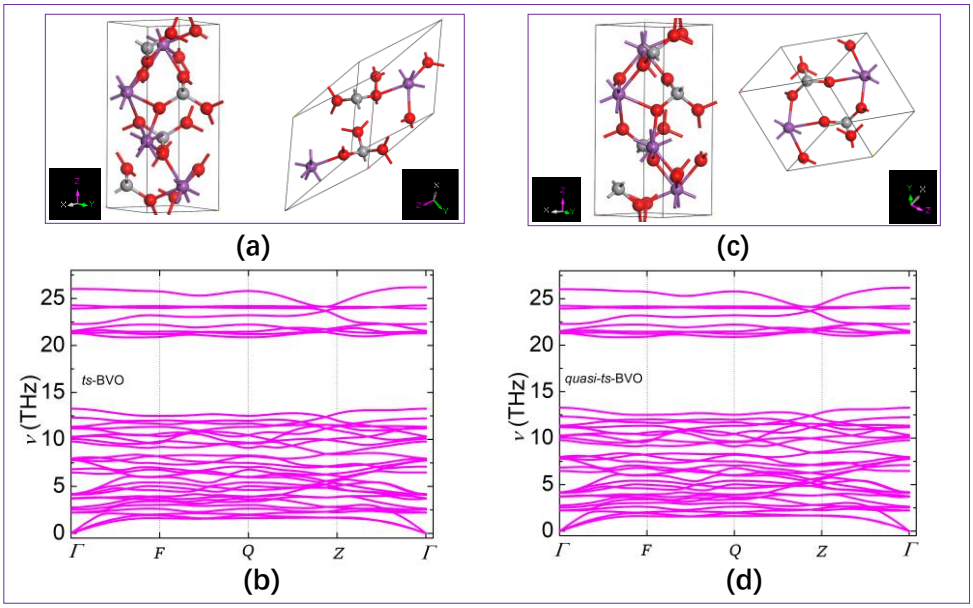

Figure 2. (a) The structure of (right) optimised primitive cell of *ts*-BVO, and (left) the common crystallographic unit cell (experimental lattice parameters a=b=5.147, c=11.722 Å) of *ts*-BVO, (b) The phonon dispersion of *ts*-BVO (c) The structure of (right) the primitive cell of *quasi-ts*-BVO optimised from *ms*-BVO, and (left) the common crystallographic unit cell (experimental lattice parameters a=5.215, b=5.084, c=11.706 Å, γ =90.394^{o}) of *ms*-BVO, and (d) The phonon dispersion of *quasi-ts*-

BVO. The high symmetry q-points are Γ (0, 0, 0), F (0, 0.5, 0), Q (0, 0.5, 0.5), and Z (0.5, 0.5, -0.5), in fractions of the reciprocal lattice vectors. The red spheres, grey spheres, and the purple spheres are O, V and Bi atoms, respectively.

Table 2. The lattice parameters and bond lengths of Bi-O and V-O of *ms*-BVO and *ts*-BVO from experiment[11] and optimized with the PBEsol functional and the hybrid functional with α=0.6 (see Methods for details).

Phases		Lattice parameters	Bi-O bond length (Å)	V-O bond length (Å)
ms-BVO	Exp.	α=β=67.911° γ =116.403° a=b=6.887 Å c=5.215 Å	2.676×2 2.533×2 2.349×2 2.314×2	1.747×2 1.739×2
	Opt.-PBEsol	α=β=67.979° γ=115.951° a=b=6.820 Å c=5.114 Å	2.457×2 2.456×2 2.420×2 2.419×2	1.733×4
	Opt-hybrid	α=β=67.934° γ=116.450° a=b=6.748 Å c=5.127 Å	2.601×2 2.477×2 2.339×2 2.297×2	1.709×2 1.693×2
ts-BVO	Exp.	α=β=136.195° γ =63.680° a=b=c=6.899 Å	2.450×4 2.494×4	1.727×4
	Opt.	α=β=135.955° γ=64.050° a=b=c=6.820 Å	2.420×4 2.458×4	1.733×4

Optimisation of the *ms*-BVO with the PBEsol functional generates a tetragonal structure as noted above. The structure is shown in **Figure 2 (c)** and structural parameters are listed in **Table 2.** The lattice parameters are close to experimental values. But the four sets of Bi-O bond lengths have insignificant differences, and there is only one set of V-O bonds. These values correspond to the tetragonal phase within the error tolerance of ~ 10^{-3} Å. In order to distinguish from *ts*-BVO, we denote it *quasi-ts*-BVO. We confirmed this finding using the FHI-aims code which employs atom-centred basis functions. Optimised 4×4×4 and 6×6×6 supercells of this *quasi-ts*-

BVO structure with 768 and 2592 atoms respectively have been used for the phonon calculation with closely matching results. The phonon dispersion with the non-analytical term correction using the 6×6×6 supercell is shown in **Figure 2 (d),** and again there are no soft modes.

Considering if more modern higher-order methods beyond the capabilities of the PBEsol and PBE functional would yield the required level of accuracy, we also used a Meta-GGA SCAN functional[46] and found that the results are similar to those from the PBEsol functional, which is also confirmed by Laraib *et al*.[47] Checking the effect of potentially viable local strong correlations, we also tried a DFT+U approach with the *U* values on V 3d and O2p states taken from our previous work [48]. On optimisation, however, the monoclinic structure still turned into tetragonal. Furthermore, we also added in turns the *U* values of 4, 7, and 10 eV on the Bi 6s state – for neither parameter, the structure retained its experimentally observed monoclinic character.

3.2 BVO calculations with hybrid functional

Next, we explore the effect of inclusion of a fraction (α ranging from 0 to 1) of the more accurate HF exchange in the DFT expression known as hybrid functionals[49]. We first optimize the *ts*-BVO with the "standard" α=0.25 increasing to 0.7. The *ts*-BVO remains tetragonal after optimization. With α=0.25, 0.4, and 0.5, there are no soft phonon modes at the gamma point. With α=0.55 and 0.6, there is a soft optical phonon mode at the gamma point with the values of 0.28*i* and 0.75*i* THz, respectively, that is represented as a negative frequency below the three acoustic modes in **Figure 3 (a)**. As well as using Phonopy, we also use the finite element method implemented in the

VASP code which reports frequency of the soft mode at the gamma point as 0.87*i* THz with α=0.6. On inspection of the irreducible representations of the modes, we found that the soft mode has a B_g symmetry. When α=0.65 and 0.7, there appear three soft optical modes. The lowest soft mode belongs to the B_g representation. The other two modes are degenerate and belong to the E_g representation. The B_g and E_g frequencies in *ts*-BVO for different values of α are shown in **Figure 3 (a).**

We next optimize the *ms*-BVO with α of 0.25 (i.e PBEsol0), 0.4, 0.5, 0.55, 0.6, 0.65 and 0.7. We also performed a calculation with the widely used HSE06 functional (with α=0.25). We found that when α is less than 0.4, the outcome of the optimisation of *ms*-BVO is still *quasi*-*ts*-BVO. This finding seems not to be consistent with previous results reported by Kweon *et al*.[50] based on constant volume calculations where the *ms*-BVO was obtained with the HSE06 (α=0.25) hybrid functional; however, in our case, we fully relax the geometry, including cell dimensions. For values of α from 0.5 to 0.7, the optimisation results in *ms*-BVO. We found that an α value of 0.6 gives a monoclinic geometry of the *ms*-BVO as shown in Table 1, which is fully consistent with experimental structure. We also calculated the phonon frequencies using the primitive cell with different values of α. The resulting two lowest B_g and one lowest A_g frequencies in *ms*-BVO are shown in **Figure 3 (b).** Moreover, we found with α=0.7, there is one soft B_u mode in *ms*-BVO.

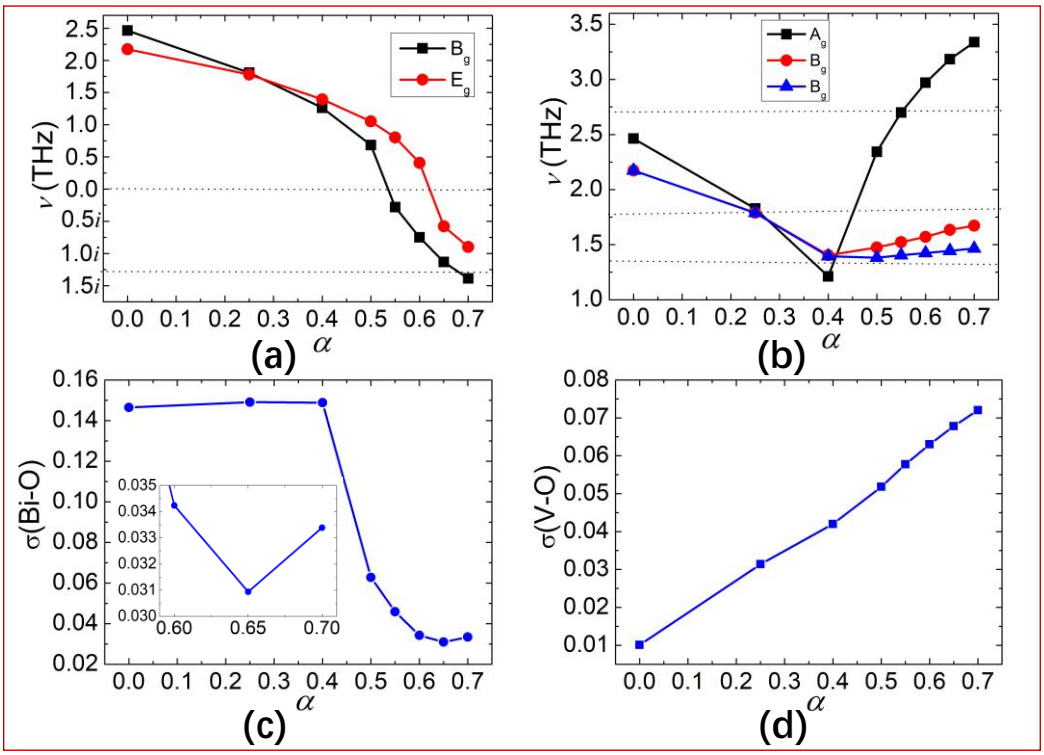

Figure 3. (a) The calculated lowest B_g and E_g frequencies in *ts*-BVO, the dotted line below 0 is the experimental value of B_g mode at 0 K. (b) The calculated two lowest B_g and one lowest A_g frequencies in *ms*-BVO; the dotted lines are the experimental values at 0 K. (c) Standard deviations of Bi-O bond length in optimized *ms*-BVO, and (d) Standard deviations of V-O bond length in optimized *ms*-BVO. Experimental phonon modes frequencies are taken from Pinczuk et al[13]. α is the fraction of HF exchange.

In order to find which value of α is most appropriate to describe the monoclinic structure, we calculated the standard deviations (SD) of the Bi-O and V-O bond lengths in optimized *ms*-BVO. The SD is defined as $\sigma = \sqrt{\frac{\sum_{i=1}^{n}(x-x_0)^2}{n}}$, where x is the bond length of Bi-O or V-O in optimised *ms*-BVO, and x_0 is the experimental Bi-O or V-O bond length. The σ(Bi-O) and σ(V-O) are shown in **Figure 3(c)** and **Figure 3 (d)**. The results for σ(Bi-O) shows that the calculated structure is close to experiment for α=0.65. But the σ(V-O) shows that the smaller values of α the closer the structure to experiment. In the displacive transition of BVO, the displacement of Bi plays a key

role. So, we consider σ(Bi-O) is the determining factor here and α ~ 0.65 is most appropriate for modelling *ms*-BVO.

The experimental work of Pinczuk et al's[13] reports one A_g and two B_g modes in the *ms*-BVO. With the phase transition from *ms*-BVO to *ts*-BVO, the A_g mode in *ms*-BVO transforms into the B_g mode in *ts*-BVO, and the two B_g modes in *ms*-BVO merge to become the E_g mode in *ts*-BVO. At 0 K, the values of these three modes in *ms*-BVO are shown in Figure 3 (b). Since the present calculations are athermal, there are nor thermal effects neither zero points vibrations included. The B_g mode becomes soft in *ts*-BVO with the value around 1.24*i* to 1.32*i* THz. In our calculations, when α is smaller than 0.5, there is no soft mode in *ts*-BVO. When α=0.7, there is a soft mode in *ms*-BVO. No experimental data indicate soft modes in *ms*-BVO showing that α should lie between 0.5 and 0.7, and we focus on the values of 0.55, 0.6 and 0.65. With α=0.65, the E_g mode becomes soft in *ts*-BVO which does not have experimental support. With α=0.55, the value of the soft B_g frequency in *ts*-BVO is only 0.28*i* THz which is far from experiment. From all these arguments, we recommend α=0.6 as optimal for describing the phase transition from *ts*-BVO to *ms*-BVO. We have noted that similar calculations with different conclusion had been reported by Kweon *et al*.[50] and Laraib *et al*.[47]. Kweon *et al*.[50] state that the conventional 25% HF admixture to the DFT exchange results in excellent agreement with experiment. They concluded that a lower 10%HF fraction failed to stabilize the monoclinic phase while a higher 50%HF fraction resulted in a significant overestimation of the monoclinic distortion. Their results required constrained relaxations which under careful examination prove

to be misleading. Laraib *et al*.[47] proposed to resolve this problem by introducing excess electrons in the conduction band of BVO by doping, which however attractive is not convincing as the levels of doping required and resultant carrier concentrations (typical of a degenerate semiconductor) are not normally reported for this system.

As described above, we use the fraction of HF exchange α in hybrid functional as a parameter to "fit" the energy ordering from experiment and found large α (~0.6) works for BVO. We didn't consider the role of entropy or electron-phonon coupling effect on the system. In fact, neither of these two factors can play a role in stabilizing the low symmetry phase of BVO, which is simply unstable on the potential energy landscape of GGA[29], meta-GGA[46] and common hybrid functionals[41] using low α values. All phonon contributions retain the hard mode nature in the low-symmetry unstable structure and do not make any difference. It is also widely accepted that the α values relates more to the electronic structure and should be chosen based on the related ground such as Koopman's condition[51] (theorem) and dielectric properties[52], we should point that this is a matter of debate in the literature. This argument is very much coming from a part of the solid-state community, the choice of α based on these grounds cannot be justified for small molecules for example, and only highlights the problem of non-transferability of α.

Originally, the hybrid functionals have been introduced in an attempt to reduce the self-interaction error in DFT and improve basic ground state properties of molecules and solids, which has been successful in many respects where better geometries and binding energies have been obtained for most known compounds only

with few notable exceptions. For a wide class of material whose valence and conduction states are localised on different chemical components of the system, band gap transitions are charge transfer processes – this is where hybrid DFT with α of about 20% has shown a dramatic improvement in the band gap prediction. This is not the case for many small molecules, where more advanced methods are required for accurate predictions of one- and two-electron processes (ionisation and excitation), that is also the case for many solids. In fact, many ground and excited state properties of materials including electron and hole localisation, optical transitions, activation energies and rates of diffusion and chemical reactions involving covalent bond breaking or formation, magnetic ordering, etc. – are commonly approached using differently tuned hybrid functionals for example using the so-called double exchange Becke's or Minnesota families of functionals[53] as we have already argued in the above section.

Finally, we investigated, in detail, the phase transition between (*quasi*-)*ts*-BVO and *ms*-BVO by modulating the tetragonal structure along the eigenvector of the soft mode with α=0.6. We use the formula $X(m)=X(0)+m\triangle X$ to describe the modulated structures, where $X(m)$ is the modulated structures, $X(0)$ is the *ts*-BVO structure, m is the displacement parameter, and $\triangle X$ is the displacement of atoms in the primitive cell along the soft mode at gamma point.

The relative energy ΔE of modulated structures *vs* m is plotted in **Figure 4 (a)**. When $m=0$, it corresponds to *ts*-BVO. As m changes, the structures distort and tend to *ms*-BVO. We found the energy curve of **Figure 4 (a)** has the form of a classical

anharmonic double-well potential which indicates the transition between *ts*-BVO and *ms*-BVO is second order in agreement with experiment[7]. The energy barrier for the transition is 0.7 meV*, which indicates that the *ts*-BVO phase may be effectively an average structure. We also show in **Figure 4 (b)** the double-well potentials calculated with a "small" plane wave basis cut-off energy of 650 eV. In this case, we determine a lower barrier of ~ 0.1 meV, but at the highly symmetric $m = 0$ point, we calculate a spuriously low total energy, which results in the *ts*-BVO phase being more stable than the *ms*-BVO phase. This result is found whether or not we include symmetry constraints in the SCF calculation; thus, the plane-wave basis cut-off of 650 eV is insufficient to describe the phase ordering of BVO, even with α=0.6. We have tested convergence of the total energy on the primitive cell of the *ms*-BVO with respect to the cut-off energy using the PBEsol functional as shown in **Figure S1** in the SI. It shows convergence of the cut-off energy only around 950 eV.

**This barrier size, which is characteristic of many displacive phase transitions, should not be directly compared to the experimental critical temperature; for a realistic comparison a full investigation of the free energy landscape with respect to appropriate order parameters would be necessary, which is beyond the scope of the current study.*

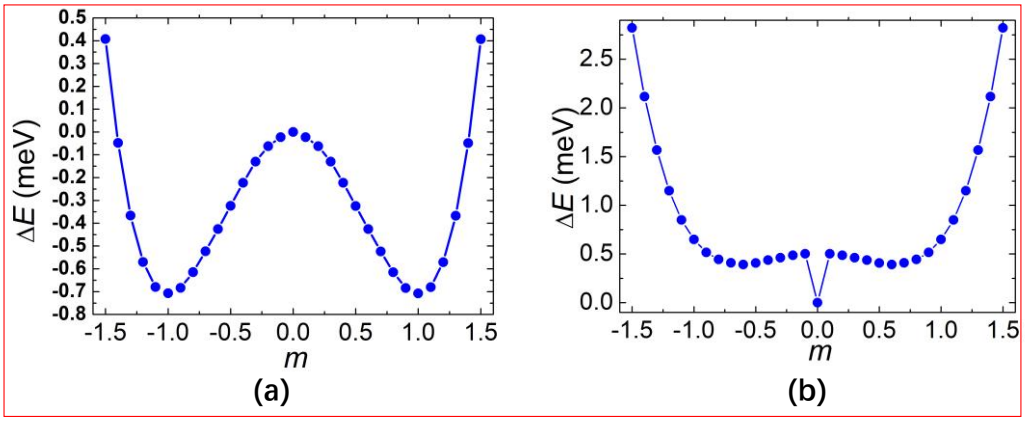

Figure 4. Anharmonic double-well potential along the soft mode at gamma point with (a) the cut-off energy of 950 eV, and (b) the cut-off energy of 650 eV.

As with other systems containing heavy elements, spin-orbit coupling (SOC) is important in BVO. We performed several PBEsol calculations including the SOC to investigate the energy ordering and stability of optimized *ms*-BVO and *ts*-BVO structures, including the phonon frequencies at the gamma point of ts-BVO; but the results show no significant difference from those without SOC. The details of these results are shown in **Figure S2** and **S3** in the SI.

We also performed calculations including SOC using the PBEsol, PBEsol0, α=0.4, α=0.5, and α=0.6 based on several points on the double-well potential. The results are shown in **Figure 5**. It is expected that the *ts*-BVO is the lowest energy using PBEsol and PBEsol0 even with the SOC corrections. The *ts*-BVO still has the lowest energy using hybrid functional even with α=0.4 and 0.5 without SOC. With SOC, for α=0.4, *ts*-BVO still has the lowest energy. For α=0.5, the SOC effect does stabilize the distorted structure but only slightly. With α=0.6, the SOC effect has lowered the energy and stabilized the distorted structure.

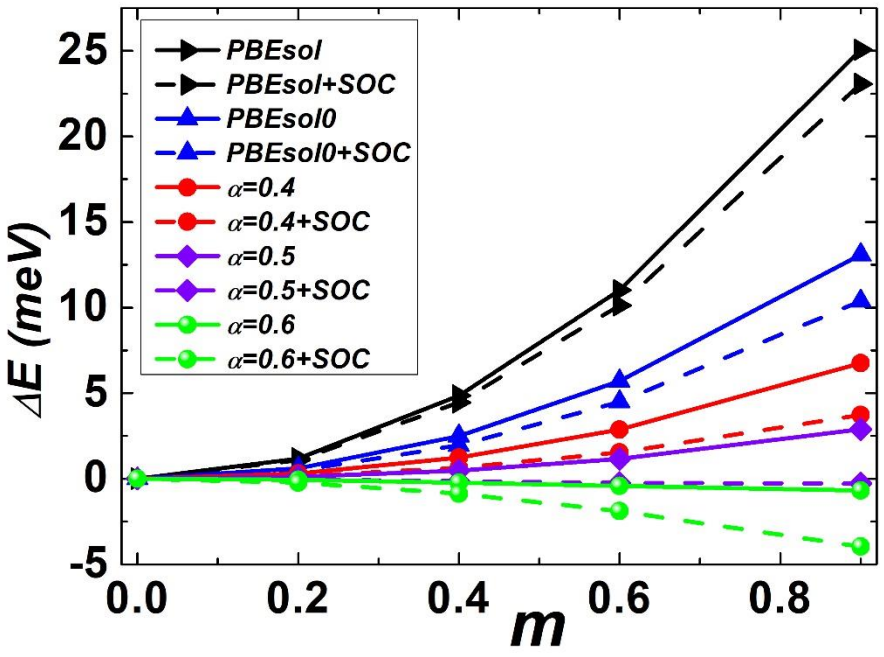

Figure 5. Energy curves of several modulated structures along the soft mode using PBEsol, PBEsol0, α=0.4, α=0.5, and α=0.6 with and without SOC effect.

3.3 PBEsol and hybrid functional on other scheelite-structured materials

In this section, we investigated selected other materials of the scheelite structural family with the PBEsol functional and hybrid functional used in our calculations on BVO that we described above. First, we performed calculations using the PBEsol functional, and the calculated energy differences are shown in **Table 3**. We find for (Sm, Pr, Y, La) NbO_4, and $YNbO_4$, the monoclinic structures have lower energy than the tetragonal phase. These materials[17-18, 23, 35] are similar as BVO which the fergusonite monoclinic structures are ferro-elastic and low temperature phase. This indicates the PBEsol functional can produce the ground state of these structures accurately. For $LuVO_4$ and $CaWO_4$, the scheelite tetragonal phase has lower energy with the PBEsol functional. For these two materials[14, 24],

the phase transition from scheelite-to-fergusonite is induced by high pressure. The scheelite tetragonal phase should be the stable phase which indicates that the PBEsol functional works well too in these two materials. But for $ScVO_4$, we find the scheelite tetragonal phase and the fergusonite monoclinic phase have almost the same energy using PBEsol functional indicating the PBEsol functional cannot distinguish these two phases. In the experiment[24, 54-56], the low-pressure zircon phase $ScVO_4$ undergoes an irreversible zircon-to-scheelite phase transition above 8.2 GPa. Beyond 18.2 GPa, it starts the scheelite-to-fergusonite phase transition. On release of pressure the fergusonite phase was detected down to 11 GPa. Below 11 GPa the sample retains the metastable phase even at ambient pressure. All these finding indicate the scheelite phase is more stable than the fergusonite phase, however, the scheelite phase may still have a small little distortion which is not observed due to thermal effects.

Since the PBEsol functional cannot distinguish the scheelite and the fergusonite phase, we then take it as an example to perform hybrid functional calculations. Based on the unit cell of the tetragonal $ScVO_4$, we construct several monoclinically distorted structures by displacing the two Sc atoms towards (or away) to each other with a step of 0.05 Å, then using the monoclinic cell setting we optimize all other geometrical parameters using the PBEsol functional. For the optimized structures, we do single point calculations using hybrid functional with α=0.25 and 0.6. The energy plot as the function of displacement of Sc using different functionals is shown in **Figure 6**. It is obviously that the little distorted

scheelite structure is becoming more and more stable with the HF exchange increase.

Table 3. The DFT energy differences of scheelite-structured ABO_4-type materials.

Materials	*E(ts-) (eV)*	*E(ms-) (eV)*	*δ[E(ts-)- E(ms-)] (eV)*
$ScVO_4$	-108.71624916	-108.71738886	0.0011
$LuVO_4$	-107.29007094	-107.28675387	-0.0033
$SmNbO_4$	-110.88526073	-110.95811368	0.0729
$PrNbO_4$	-110.54665351	-110.60848729	0.0618
$YNbO_4$	-110.45240017	-114.85662455	4.4042
$LaNbO_4$	-111.40546747	-111.48119007	0.0757
$YTaO_4$	-120.15048020	-120.34198818	0.1915
$CaWO_4$	-105.43729445	-105.42843104	-0.0089

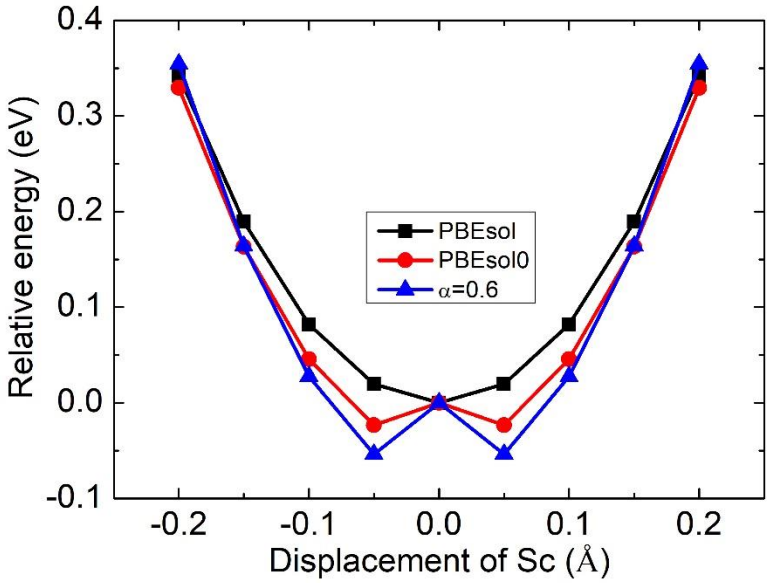

Figure 6. The energy curve with the function of displacement of Sc using different functionals.

3.4 Discussion

In the case of BVO, we found although functionals with ~ 60%HF exchange are capable of giving the correct description of the ground state of BVO, they do not give a good description of excited states in the one-electron approximation of the band structure.[50, 57] Clearly, calculations of the structure, properties and lattice dynamics of the compound need high fractions of the exact exchange interaction. The probable reason is the need to describe accurately the Bi 6s lone pair electrons which are not only needed in phonon calculations as David and Wood[9] argue, but are also crucial in determining the geometry of BVO. This also can be gleaned from the polarizability of the material. We plot the electronic density of states (DOS) calculated with PBEsol, and hybrid functionals using α=0.25, 0.6, and 0.65 in **Figure 7**. The fundamental band gap of BVO is between O 2p and V 3d states. Using PBEsol we calculate this gap to be 2.2 eV which is close to experiment[58] (~2.4 eV), indicating the PBEsol functional

can describe the polarizability of O accurately. The polarizability of Bi in turn will include an on-site contribution from a hybridization of its 6s and 6p states, and the charge transfer from Bi 6s to V 3d (mediated by O 2p states). The on-site contribution is notably underestimated with PBEsol (cf. a 13.5 eV calculated gap and experimental value of 15 eV), whereas the charge transfer mechanism, which is determined by a gap of 11.5 eV, is well described[58]. Hybrid functionals, however, gave a much poorer description of these gaps and require at least SOC corrections included in the consideration[57]. These results contrast with gas phase polarizability calculations with the details are shown in SI. In the gas phase, the polarizability of Bi^{3+} which is shown in **Table S1** in the SI is described well with PBE0 functional while in the BVO material it may be described using hybrid functional with large fractions of HF exchange.

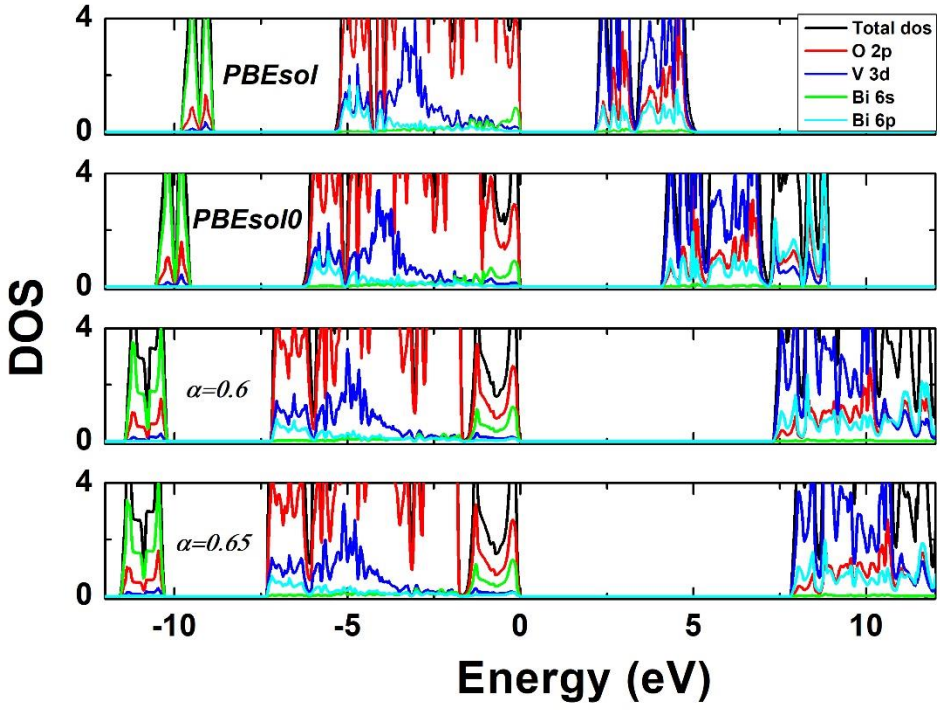

Figure 7. Electronic DOS of *ms*-BVO, the Fermi level is set at the valence band

maximum (VBM).

Furthermore, perhaps, crucially, relative sizes of constituent atoms in BVO play an important role in the phase transition. The V-O bonds remain nearly constant, and we find only small standard deviations between experiment and theory using either PBEsol or hybrid functional calculations indicating that the sizes of O and V are described to sufficient accuracy. Rigidity of VO_4 tetrahedra in the phase transition has been observed experimentally[9]. For Bi, its position off centre from BiO_8 dodecahedra play a key role in the phase transition. The overall stability of *ts*-BVO and absence of soft modes revealed by PBEsol calculations means that the Bi^{3+} ions prove to be too large to move off centre in *ts*-BVO. Standard hybrid functionals like PBEsol0, PBE0, and HSE06 (with α=0.25) are commonly expected to perform well for average atomic structures and band gaps, but as we found can still fail, as in the present case, when tackling heavy elements, such as Bi. A different weight of the HF exchange is required to reproduce or predict different observables, as a general rule, and, a higher fraction of the HF exchange than 25% is required in the solid state, as pointed out by Cora et al.[59]. On increasing the HF exchange fraction α from 0 to 50%, there is still no soft modes in *ts*-BVO meaning that the Bi^{3+} radius is still too large. The effective radii of the Bi^{3+} and O^{2-} ions changing with α are shown in the inserted graph in the **Figure 8**. The effective radii of the Bi^{3+} and O^{2-} ions have been obtained from the charge density graphs as distances from the respective nuclei to the density minimum on the Figure 8. On the Figure, Bi is on the left, and O is on the right. The insert figure clearly shows the ion reduction with α. We have concentrated on the Bi ion in this

analysis as the reduction of O is a common effect in all materials of this class, but only BVO proves to be problematic for common DFT approaches. Increasing α further above 50%, the Bi^{3+} ions become sufficiently small and move readily off centre in the BiO_8 dodecahedra, which explains why we could describe the phase transition in BVO with 60%HF. This behaviour can be attributed to the disbalance in the self-interaction error when describing valence O 2p and Bi 6s lone pair electrons.

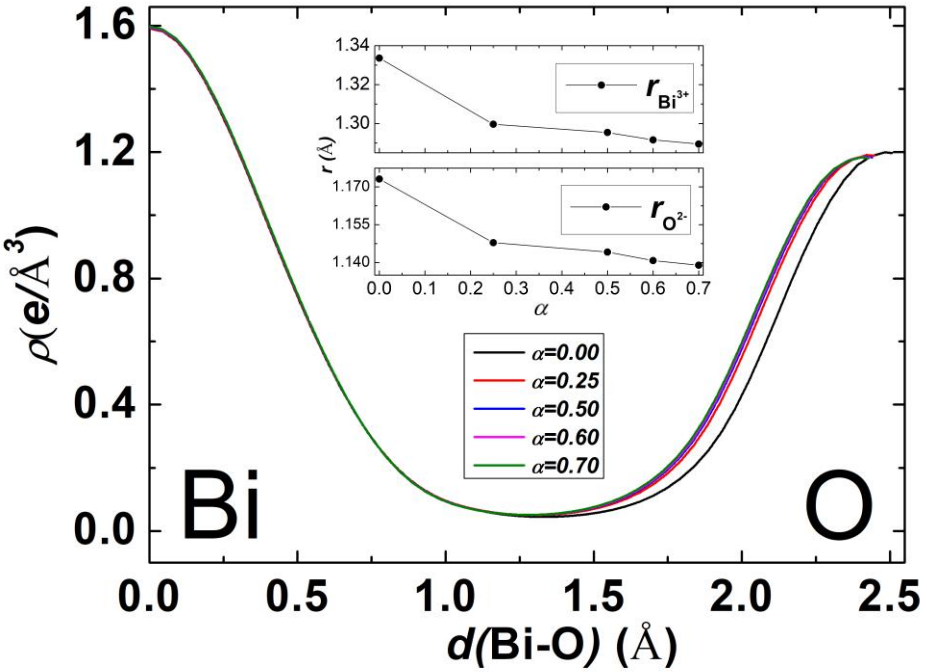

Figure 8. Charge density line profile ρ in unit of e/Å^3 along the longer Bi-O bond in the tetragonal phase of BVO. The inserted graph is the effective radii of the Bi^{3+} and O^{2-} ions change with α.

4. Conclusion

A number of popular local, semi-local, and hybrid functionals with low fractions of HF exchange (≤ 25%) in DFT are widely used and accepted when simulating the properties of materials. Here, we demonstrate, that the basic ground state structure

and phonon properties of BVO can only be described using a hybrid DFT with an unusually larger fraction of ~60% HF under extremely high convergence criteria. In other scheelite-structured ABO_4 materials which adopts both scheelite and fergusonite symmetry, we observe a similar behaviour with the ground state not reproduced correctly for some of them. In general, based on this work and what we find in the literature, we find that $LaNbO_4$ are already described well by LDA; $YTaO_4$ and $HoTaO_4$ by PBE; $HoNbO_4$, $SmNbO_4$ and $SmTaO_4$ by PBEsol. While in BVO and $ScVO_4$, the calculations do require over 50% of the HF exchange. Considering recent double hybrid DFT approaches that typically employ high fractions of the HF exchange along with the MP2-type or similar expressions for the nonlocal correlation contributions[53], we might expect that the problem of finding a unified approach to the whole class of the material lies in the missing nonlocal correlation functional absent in the current generation of popular density functional methods.

Our results not only give a fundamental understanding of the phase transition in BVO but also indicate the challenges which may face standard DFT or hybrid DFT with only low fractions of HF when investigating structure and physical properties of materials, especially those with highly polarisable ions. Our findings for BVO are directly relevant for the studies of phase transition in ABO_4-type materials showing scheelite tetragonal to fergusonite monoclinic structural transformations.

ASSOCIATED CONTENT

Supporting information

The supporting information includes: Planewave cut-off energy test; Spin-orbit coupling effect on potential energy landscape of BVO and on the phonon frequencies of ts-BVO; The details of gas phase Bi^{3+} polarizability calculations using NWChem code; The details of FHI-AIMS input.

Corresponding Authors

T. Liu: uccatl0@ucl.ac.uk;
A. Sokol: a.sokol@ucl.ac.uk;
J. Buckeridge: j.buckeridge@lsbu.ac.uk

Notes

The authors declare no competing financial interests.

ACKNOWLEDGMENTS

The authors acknowledge funding from EPSRC Grants EP/I01330X/1, EP/K016288/1, and EP/N01572X/1. The authors also acknowledge the use of the UCL Thomas, Faraday, Kathleen, and Grace High Performance Computing Facilities (Thomas@UCL, Faraday@UCL, Kathleen@UCL, and Grace@UCL) and associated support services, and the ARCHER and ARCHER2 supercomputers through membership of the UK's HPC Materials Chemistry Consortium, which is funded by EPSRC Grant EP/R029431, EP/P020194, in the completion of this work. T. L. acknowledges support from the National Natural Science Foundation of China (grants 21703054 and 22173026) and Henan University's Engineering Research Center for Nanomaterials (ERCN) and International Affairs Office.

Author contribution

All authors contributed to the study reported in this paper. T. L. carried out the calculations and written the manuscript; J. B. helped with the calculation details and discussion of the results and edited the manuscript. A.W. provided useful suggestions and made important contributions to the discussion. A.A.S. gave the idea of the work and led the project. C.R.A.C. supervised the project and edited the manuscript. X. Z. performed the NWChem calculations. J.C. provided scripts for eigenvector scanning.

REFERENCES

1. Park, Y.; McDonald, K. J.; Choi, K.-S., Progress in Bismuth Vanadate Photoanodes for Use in Solar Water Oxidation. *Chem. Soc. Rev.* **2013**, *42*, 2321-2337.
2. Abdi, F. F.; Berglund, S. P., Recent Developments in Complex Metal Oxide Photoelectrodes. *J. Phys. D: Appl. Phys.* **2017**, *50*, 193002.
3. Tayebi, M.; Lee, B.-K., Recent Advances in Bivo4 Semiconductor Materials for Hydrogen Production Using Photoelectrochemical Water Splitting. *Renew. Sust. Energ. Rev.* **2019**, *111*, 332-343.
4. Wang, Z.; Huang, X.; Wang, X., Recent Progresses in the Design of $BiVO_4$-Based Photocatalysts for Efficient Solar Water Splitting. *Catal. Today* **2019**, *335*, 31-38.
5. Kudo, A.; Omori, K.; Kato, H., A Novel Aqueous Process for Preparation of Crystal Form-Controlled and Highly Crystalline $BiVO_4$ Powder from Layered Vanadates at Room Temperature and Its Photocatalytic and Photophysical Properties. *J. Am. Chem. Soc.* **1999**, *121*, 11459-11467.
6. Li, R.; Zhang, F.; Wang, D.; Yang, J.; Li, M.; Zhu, J.; Zhou, X.; Han, H.; Li, C., Spatial Separation of Photogenerated Electrons and Holes among {010} and {110} Crystal Facets of $BiVO_4$. *Nat. Commun.* **2013**, *4*, 1-7.
7. Bierlein, J.; Sleight, A., Ferroelasticity in $BiVO_4$. *Solid State Commun.* **1975**, *16*, 69-70.
8. David, W.; Glazer, A.; Hewat, A., The Structure and Ferroelastic Phase Transition of $BiVO_4$. *Phase Transitions: A Multinational Journal* **1979**, *1*, 155-169.
9. David, W.; Wood, I., Ferroelastic Phase Transition in $BiVO_4$: V. Temperature Dependence of Bi^{3+} Displacement and Spontaneous Strains. *J. Phys. C: Solid State Phys.* **1983**, *16*, 5127.
10. David, W.; Wood, I., Ferroelastic Phase Transition in $BiVO_4$: Vi. Some Comments on the Relationship between Spontaneous Deformation and Domain Walls in Ferroelastics. *J. Phys. C: Solid State Phys.* **1983**, *16*, 5149.
11. Sleight, A.; Chen, H.-Y.; Ferretti, A.; Cox, D., Crystal Growth and Structure of $BiVO_4$. *Mater. Res. Bull.* **1979**, *14*, 1571-1581.
12. Pinczuk, A.; Welber, B.; Dacol, F., Mechanism of the Ferroelastic Transition of $BiVO_4$. *Solid State Commun.* **1979**, *29*, 515-518.
13. Pinczuk, A.; Burns, G.; Dacol, F., Soft Optical Phonon in Ferroelastic $BiVO_4$. *Solid State Commun.* **1977**, *24*, 163-165.
14. Errandonea, D.; Manjón, F. J., On the Ferroelastic Nature of the Scheelite-to-Fergusonite Phase Transition in Orthotungstates and Orthomolybdates. *Mater. Res. Bull.* **2009**, *44*, 807-811.
15. Errandonea, D.; Manjón, F. J., Pressure Effects on the Structural and Electronic Properties of ABX_4 Scintillating Crystals. *Progress in Materials Science* **2008**, *53*, 711-773.
16. Popolitov, V.; Ivanova, L.; Stephanovitch, S. Y.; Chetchkin, V.; Lobachev, A.; Venevtsev, Y. N., Ferroelectrics ABO_4: Synthesis of Single Crystals and Ceramics; Dielectric and Nonlinear Optical Properties. *Ferroelectrics* **1974**, *8*, 519-520.
17. Nikiforova, G.; Khoroshilov, A.; Gavrichev, K.; Knyazev, A.; Knyazeva, S., Fergusonite–Scheelite Phase Transition of Praseodymium Orthoniobate. *Inorg. Mater.* **2019**, *55*, 964-967.
18. Huse, M.; Skilbred, A. W. B.; Karlsson, M.; Eriksson, S. G.; Norby, T.; Haugsrud, R.; Knee, C. S., Neutron Diffraction Study of the Monoclinic to Tetragonal Structural Transition in $LaNbO_4$ and Its Relation to Proton Mobility. *J. Solid State Chem.* **2012**, *187*, 27-34.
19. Fjeld, H.; Toyoura, K.; Haugsrud, R.; Norby, T., Proton Mobility through a Second Order Phase Transition: Theoretical and Experimental Study of $LaNbO_4$. *Phys. Chem. Chem. Phys.* **2010**, *12*, 10313-

10319.
20. Arulnesan, S. W.; Kayser, P.; Kimpton, J. A.; Kennedy, B. J., Studies of the Fergusonite to Scheelite Phase Transition in $LnNbO_4$ Orthoniobates. *J. Solid State Chem.* **2019**, *277*, 229-239.
21. Auckett, J. E.; Lopez-Odriozola, L.; Clark, S. J.; Evans, I. R., Exploring the Nature of the Fergusonite–Scheelite Phase Transition and Ionic Conductivity Enhancement by Mo^{6+} Doping in $LaNbO_4$. *J. Mater. Chem. A* **2021**, *9*, 4091-4102.
22. Aldred, A., Cell Volumes of APO_4, AVO_4, and $ANbO_4$ Compounds, Where a= Sc, Y, La–Lu. *Acta Crystallographica Section B: Structural Science* **1984**, *40*, 569-574.
23. Sarin, P.; Hughes, R. W.; Lowry, D. R.; Apostolov, Z. D.; Kriven, W. M., High‐Temperature Properties and Ferroelastic Phase Transitions in Rare‐Earth Niobates ($LnNbO_4$). *J. Am. Ceram. Soc.* **2014**, *97*, 3307-3319.
24. López-Solano, J.; Rodríguez-Hernández, P.; Muñoz, A., Ab Initio Study of High-Pressure Structural Properties of the Luvo4 and $ScVO_4$ Zircon-Type Orthovanadates. *High Pressure Research* **2009**, *29*, 582-586.
25. Kondrat'eva, O.; Nikiforova, G.; Tyurin, A.; Ryumin, M.; Gurevich, V.; Kritskaya, A.; Gavrichev, K., Calorimetric Study of Ytterbium Orthovanadate $YbVO_4$ Polycrystalline Ceramics. *Ceramics International* **2018**, *44*, 18103-18107.
26. Errandonea, D.; Lacomba-Perales, R.; Ruiz-Fuertes, J.; Segura, A.; Achary, S. N.; Tyagi, A. K., High-Pressure Structural Investigation of Several Zircon-Type Orthovanadates. *Phy. Rev. B* **2009**, *79*, 184104.
27. Feng, J.; Shian, S.; Xiao, B.; Clarke, D. R., First-Principles Calculations of the High-Temperature Phase Transformation in Yttrium Tantalate. *Phy. Rev. B* **2014**, *90*, 094102.
28. Levin, I., Nist Inorganic Crystal Structure Database (Icsd). National Institute of Standards and Technology: 2018.
29. Perdew, J. P.; Burke, K.; Ernzerhof, M., Generalized Gradient Approximation Made Simple. *Phy. Rev. Lett.* **1996**, *77*, 3865.
30. Blokhin, E.; Gryaznov, D.; Kotomin, E.; Evarestov, R.; Maier, J., A Comparative Hybrid DFT Study of Phonons in Several $SrTiO_3$ Phases. *Integr. Ferroelectr.* **2011**, *123*, 18-25.
31. Xie, Y.; Yu, H.-t.; Zhang, G.-x.; Fu, H.-g., Lattice Dynamics Investigation of Different Transition Behaviors of Cubic $BaTiO_3$ and $SrTiO_3$ by First-Principles Calculations. *J. Phys.: Condens. Matter* **2008**, *20*, 215215.
32. Heifets, E.; Kotomin, E.; Trepakov, V. A., Calculations for Antiferrodistortive Phase of $SrTiO_3$ perovskite: Hybrid Density Functional Study. *J. Phys.: Condens. Matter* **2006**, *18*, 4845-4851.
33. Zhang, Q.; Cagin, T.; Goddard, W. A., The Ferroelectric and Cubic Phases in $BaTiO_3$ Ferroelectrics Are Also Antiferroelectric. *Proc. Natl. Acad. Sci. U.S.A.* **2006**, *103*, 14695-14700.
34. Chen, Z.-X.; Chen, Y.; Jiang, Y.-S., Dft Study on Ferroelectricity of $BaTiO_3$. *J. Phys. Chem. B* **2001**, *105*, 5766-5771.
35. Mullens, B. G.; Avdeev, M.; Brand, H. E. A.; Mondal, S.; Vaitheeswaran, G.; Kennedy, B. J., Insights into the Structural Variations in $SmNb_{1-x}Ta_xO_4$ and $HoNb_{1-x}Ta_xO_4$ Combined Experimental and Computational Studies. *Dalton Transactions* **2021**, *50*, 9103-9117.
36. Csonka, G. I.; Perdew, J. P.; Ruzsinszky, A.; Philipsen, P. H.; Lebègue, S.; Paier, J.; Vydrov, O. A.; Ángyán, J. G., Assessing the Performance of Recent Density Functionals for Bulk Solids. *Phy. Rev. B* **2009**, *79*, 155107.
37. Kuwabara, A.; Haugsrud, R.; Stølen, S.; Norby, T., Local Condensation around Oxygen Vacancies in T-$LaNbO_4$ from First Principles Calculations. *Phys. Chem. Chem. Phys.* **2009**, *11*, 5550-5553.

38. Evarestov, R. A.; Bandura, A. V., First‐Principles Calculations on the Four Phases of $BaTiO_3$. *J. Comput. Chem.* **2012**, *33*, 1123-1130.
39. Kresse, G.; Furthmüller, J., Efficient Iterative Schemes for Ab Initio Total-Energy Calculations Using a Plane-Wave Basis Set. *Phy. Rev. B* **1996**, *54*, 11169.
40. Kresse, G.; Furthmüller, J., Efficiency of Ab-Initio Total Energy Calculations for Metals and Semiconductors Using a Plane-Wave Basis Set. *Comput. Mater. Sci.* **1996**, *6*, 15-50.
41. Adamo, C.; Barone, V., Toward Reliable Density Functional Methods without Adjustable Parameters: The PBE0 Model. *J. Chem. Phys.* **1999**, *110*, 6158-6170.
42. Blum, V.; Gehrke, R.; Hanke, F.; Havu, P.; Havu, V.; Ren, X.; Reuter, K.; Scheffler, M., Ab Initio Molecular Simulations with Numeric Atom-Centered Orbitals. *Comput. Phys. Commun.* **2009**, *180*, 2175-2196.
43. Togo, A.; Oba, F.; Tanaka, I., First-Principles Calculations of the Ferroelastic Transition between Rutile-Type and $CaCl_2$-Type SiO_2 at High Pressures. *Phy. Rev. B* **2008**, *78*, 134106.
44. Togo, A.; Tanaka, I., First Principles Phonon Calculations in Materials Science. *Scripta Mater.* **2015**, *108*, 1-5.
45. Jain, A., et al., Commentary: The Materials Project: A Materials Genome Approach to Accelerating Materials Innovation. *APL Materials* **2013**, *1*, 011002.
46. Sun, J.; Remsing, R. C.; Zhang, Y.; Sun, Z.; Ruzsinszky, A.; Peng, H.; Yang, Z.; Paul, A.; Waghmare, U.; Wu, X., Accurate First-Principles Structures and Energies of Diversely Bonded Systems from an Efficient Density Functional. *Nature chemistry* **2016**, *8*, 831-836.
47. Laraib, I.; Carneiro, M. A.; Janotti, A., Effects of Doping on the Crystal Structure of $BiVO_4$. *J. Phys. Chem. C* **2019**, *123*, 26752-26757.
48. Liu, T.; Zhao, Q.; Li, C.; Lyu, Y.; Dupuis, M., Photocatalytic Facet Selectivity in $BiVO_4$ Nanoparticles: Polaron Electronic Structure and Thermodynamic Stability Considerations for Photocatalysis. *J. Phys. Chem. C* **2019**, *123*, 20142-20151.
49. Becke, A. D., A New Mixing of Hartree‐Fock and Local Density‐Functional Theories. *J. Chem. Phys.* **1993**, *98*, 1372-1377.
50. Kweon, K. E.; Hwang, G. S., Hybrid Density Functional Study of the Structural, Bonding, and Electronic Properties of Bismuth Vanadate. *Phy. Rev. B* **2012**, *86*, 165209.
51. Koopmans, T., Über Die Zuordnung Von Wellenfunktionen Und Eigenwerten Zu Den Einzelnen Elektronen Eines Atoms. *Physica* **1934**, *1*, 104-113.
52. Wang, W.; Strohbeen, P. J.; Lee, D.; Zhou, C.; Kawasaki, J. K.; Choi, K.-S.; Liu, M.; Galli, G., The Role of Surface Oxygen Vacancies in $BiVO_4$. *Chem. Mater.* **2020**, *32*, 2899-2909.
53. Stein, F.; Hutter, J.; Rybkin, V. V., Double-Hybrid Dft Functionals for the Condensed Phase: Gaussian and Plane Waves Implementation and Evaluation. *Molecules* **2020**, *25*.
54. Panchal, V.; Manjón, F. J.; Errandonea, D.; Rodriguez-Hernandez, P.; López-Solano, J.; Muñoz, A.; Achary, S. N.; Tyagi, A. K., High-Pressure Study of $ScVO_4$ by Raman Scattering and Ab Initio Calculations. *Phy. Rev. B* **2011**, *83*, 064111.
55. Garg, A. B.; Errandonea, D.; Rodríguez-Hernández, P.; Muñoz, A., Scvo4under Non-Hydrostatic Compression: A New Metastable Polymorph. *J. Phys.: Condens. Matter* **2016**, *29*, 055401.
56. Sheng, S.-F., Pressure-Induced Phase Transition for $ScVO_4$: A First-Principles Study. *Physica B: Condensed Matter* **2013**, *426*, 20-23.
57. Wiktor, J.; Reshetnyak, I.; Ambrosio, F.; Pasquarello, A., Comprehensive Modeling of the Band Gap and Absorption Spectrum of $BiVO_4$. *Phy. Rev. Mater.* **2017**, *1*, 022401.

58. Cooper, J. K.; Gul, S.; Toma, F. M.; Chen, L.; Glans, P.-A.; Guo, J.; Ager, J. W.; Yano, J.; Sharp, I. D., Electronic Structure of Monoclinic $BiVO_4$. *Chem. Mater.* **2014**, *26*, 5365-5373.
59. Corà, F.; Alfredsson, M.; Mallia, G.; Middlemiss, D. S.; Mackrodt, W. C.; Dovesi, R.; Orlando, R., The Performance of Hybrid Density Functionals in Solid State Chemistry. In *Principles and Applications of Density Functional Theory in Inorganic Chemistry Ii*, Kaltsoyannis, N.; McGrady, J. E., Eds. Springer Berlin Heidelberg: Berlin, Heidelberg, 2004; pp 171-232.

TOC

Anharmonic double-well potential for the phase transition from *ms*-BVO to *ts*-BVO along the soft mode at gamma point of ts-BVO.